






RESEARCH ARTICLE | AUGUST 20 2024

Numerical investigation of a three-dimensional flow structure influenced by the lateral expansion of a partially distributed submerged canopy

Si-Yuan Song (宋思源) ; Xie-Kang Wang (王协康); Huan-Feng Duan (段焕丰) ; Alessandro Stocchino ; Xu-Feng Yan (闫旭峰)  



Physics of Fluids 36, 085164 (2024)

<https://doi.org/10.1063/5.0221723>



Articles You May Be Interested In

Evaluation of the aerodynamic loads over isolated and clustered tree canopies using large eddy simulation

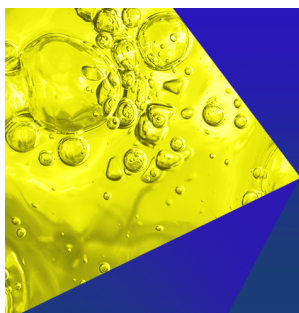
Physics of Fluids (April 2025)

Large-eddy simulation of an open-channel flow bounded by a semi-dense rigid filamentous canopy: Scaling and flow structure

Physics of Fluids (June 2019)

Effect of waves on current over staggered cylindrical canopies

Physics of Fluids (June 2025)



Physics of Fluids
Special Topics
Open for Submissions

[Learn More](#)

Numerical investigation of a three-dimensional flow structure influenced by the lateral expansion of a partially distributed submerged canopy

Cite as: Phys. Fluids **36**, 085164 (2024); doi: 10.1063/5.0221723

Submitted: 3 June 2024 · Accepted: 28 July 2024 ·

Published Online: 20 August 2024



View Online



Export Citation



CrossMark

Si-Yuan Song (宋思源),¹ Xie-Kang Wang (王协康),¹ Huan-Feng Duan (段焕丰),² Alessandro Stocchino,² and Xu-Feng Yan (闫旭峰)^{1,a)}

AFFILIATIONS

¹State Key Laboratory of Hydraulics and Mountain River Engineering, Sichuan University, Chengdu, China

²Department of Civil and Environment Engineering, The Hong Kong Polytechnic University, Hong Kong, China

^{a)}Author to whom correspondence should be addressed: xufeng.yan@scu.edu.cn

ABSTRACT

This study employed numerical simulations to investigate the three-dimensional hydrodynamic structure of a channel obstructed by submerged rigid canopies. After validating the model using existing experimental data, a series of numerical experiments varying the canopy density and the blocking ratio were conducted. The results indicate that submerged canopy, different from emergent canopies, triggers the generation of three-dimensional coherent vortices. When canopies expand laterally, the scale, location, and evolution characteristics of cross-sectional secondary flows vary. The direction of secondary circulation at the canopy top of the fully covered vegetation channel is affected by the river width/depth ratio. Three-dimensional coherent vortices are jointly controlled by vertical and transverse Reynolds stresses. When the channel is seriously blocked, the degree of momentum exchange in the mixing layer does not change significantly. The boundary friction effect dominates the momentum exchange process near the wall. An equation coupling the drag length scale and blocking ratio with the vertical coherent vortex penetration length is proposed, indicating that the penetration length increases exponentially with both variables. Higher canopy density exhibits a stronger resistance to the vertical coherent vortex penetration length. In the process of canopy lateral expansion, the evolution time of the outer vortex to scale stability is longer than that of the inner vortex. The significance of research on the three-dimensional vortex structure of rigid submerged vegetation is established based on previous studies and existing conclusions.

Published under an exclusive license by AIP Publishing. <https://doi.org/10.1063/5.0221723>

I. INTRODUCTION

Riparian vegetation typically plays a crucial role in the restoration and stability of river ecosystems, the rehabilitation and protection of river channels, and water resources management.^{1–5} The obstruction caused by vegetation affects the natural flow structure of the river channel, resulting in reduced dispersion of pollutants.^{1,2} Moreover, the presence of emergent or submerged vegetation proved to strongly impact the sediment fluxes and, thus, the morphodynamics evolution of a natural channel.^{3–5} In natural context, vegetation coverage can vary in time and space, especially on river banks or floodplains.^{6,7} However, the spatial and temporal variability of vegetation is influenced by factors such as hydrology and climate, which can lead to varying degrees of channel obstruction.^{8,9}

The unevenness of emergent vegetation, partially obstructing the channel, has been extensively studied and linked to the main hydrodynamic features (secondary flows and coherent vortices), as well as river

channel morphodynamics.^{10–12} For submerged vegetation, coherent vortex structures coexist in different dimensions.¹³ Consequently, the lateral expansion of canopies can indeed lead to changes in both lateral and vertical vortex structures. Lateral vortices typically form at the edges of vegetation patches, and there is generally no significant difference between emergent and submerged vegetation in this regard. However, the vertical vortices are unique to submerged vegetation and play a crucial role in controlling the vertical momentum and mass exchange processes.^{13,14}

When water flows over the submerged canopy top, it experiences strong shear forces, leading to the occurrence of pronounced Kelvin–Helmholtz instability near that location. Furthermore, the instability induces large-scale vortices that rotate along the vertical direction.¹⁵ Subsequently, this phenomenon is commonly referred to as vertical coherent vortices. The distance from the canopy top to the bottom of the vertical coherent vortices, where these vortices partially penetrate

into the vegetation, is known as the vertical coherent vortex penetration length. Similarly, coherent vortices can also form near the lateral boundaries of the vegetation region.¹⁰ Ghisalberti and Nepf¹⁵ suggested that the size of the vertical coherent vortices grew downstream and the penetration length of these vortices increased significantly after the occurrence of Kelvin–Helmholtz instability, under the influence of the surrounding flow. However, the study did not specifically address the impact of the lateral expansion of canopies on the behavior of the vertical coherent vortices. Nepf *et al.*¹⁶ proposed a formula for predicting the vertical coherent vortex penetration length in flexible vegetation and conducted experimental validation. They identified several factors that influence the penetration length. So far, the impact of the blocking ratio on the generation and evolution of vertical coherent structures has not been thoroughly investigated. A detailed description of these processes and the effect of lateral canopy expansion is one of the main purposes of this study.

Consideration of cross-sectional secondary circulation structures is still limited compared to the three-dimensional coherent vortices generated by water flow over the top and lateral edge of the canopy, especially in the context of changing the blocking ratio. Choi and Kang¹⁷ simulated the flow structure in partially vegetated channels and explored the effects of canopy density on the evolution of secondary flows. Secondary flows have a significant impact on the transport processes of pollutants and sediments in rivers, which is comparable to the influence of three-dimensional coherent vortices.¹⁸ Shi *et al.*¹⁹ conducted simulations to investigate the secondary flow structures in narrow open channels under the influence of submerged vegetation. They suggested a correlation between the circulation patterns and the distinctive S-shaped velocity profiles. Moreover, the connection between secondary flows and coherent vortices is still an open question.

Nepf and Vivoni²⁰ defined the distance between the vertical location where the Reynolds stress decays to 10% of its peak and the canopy top as the penetration length δ_e . Nepf *et al.*¹⁶ proposed a formula for predicting the flexible vegetation penetration length,

$$\frac{\delta_e}{h} \approx \frac{0.23 \pm 0.06}{C_d a h}, \quad (1)$$

where $C_d a h = 0.1$ – 0.23 , indicating that the canopy-scale vortices penetrate the canopy completely. However, when $C_d a h$ values are larger, the generated vortices do not fully penetrate the canopy. Ghisalberti and Nepf¹⁵ proposed that the significant mass and momentum exchange in the mixing layer near the canopy top generates coherent vertical vortices that penetrate into the vegetation region. These vortices can be defined by the longitudinal velocity distribution (see Fig. 1).

To further control variables for subsequent analysis, we propose to use the velocity distribution at the midpoint of the current vegetation region as the standard for determining the location of vertical coherent vortex generation. Thereby consistency can be ensured and variables can be analyzed in a more targeted manner.

II. METHODOLOGY

A. Numerical model

We implemented a specific three-dimensional hydrodynamic solver, namely Nays CUBE, which allows for a detailed description of the secondary flows by implementing different turbulent closure models. This hydrodynamic solver has been successfully applied to river applications, e.g., to study the morphodynamics and local scour

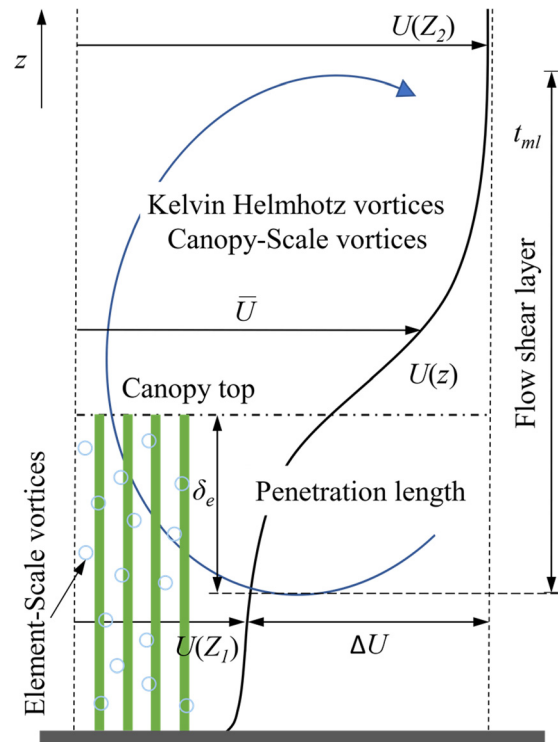


FIG. 1. Characteristic velocity and length scales in a central vegetation region. $\Delta U = U(Z_2) - U(Z_1)$, where $U(Z_1)$ and $U(Z_2)$ are the low- and high-stream velocities, respectively. $U(z) - U(Z_1) = 0.1\Delta U$. $\delta_e = h - Z$, where h is the canopy height.

dynamics²¹ or the three-dimensional flow structures in a realistic case study.²² In particular, we implemented the RANS equation approach using a second-order k-epsilon model. The governing equations of the model are given as follows:

Continuity equation,

$$\frac{\partial U_i}{\partial x_i} = 0, \quad (2)$$

where x_i is the spatial coordinates and U_i is the time-averaged velocity components.

Momentum equation,

$$\frac{\partial U_i}{\partial t} + \frac{\partial U_i U_j}{\partial x_j} = \delta_{i3} g - \frac{1}{\rho} \left(\frac{\partial p}{\partial x_i} + F_{dr}^i \right) + \frac{\partial (-\overline{u_i' u_j'})}{\partial x_j} + \nu \frac{\partial^2 U_i}{\partial x_j \partial x_j}, \quad (3)$$

where ρ is the fluid density, g is the acceleration of gravity, p is the pressure, $-\overline{u_i' u_j'}$ is the Reynolds stress tensor, F_{dr}^i is the resistance force component (F_x, F_y, F_z) induced by the vegetation per unit volume in the x , y , and z directions, respectively, and δ_{ij} is the Kronecker symbol. The drag force term is modeled by employing the quadratic friction law,

$$F_{dr}^i = \frac{1}{2} n \rho C_d b_e u_i \sqrt{u_j u_j}, \quad (4)$$

where u_i is the velocity components, C_d is the stem drag coefficient, b_e is the effective stem width (i.e., diameter of a cylinder), and n is the stem density. C_d in the present simulation is taken as 1.5, in Sec. II B.

The equations of the k - ε model are as follows:
 k equation,

$$\frac{\partial k}{\partial t} + \frac{\partial k U_j}{\partial x_j} = -\overline{u_i' u_j'} \frac{\partial U_i}{\partial x_j} + \frac{\partial}{\partial x_j} \left[\left(\frac{\nu_t}{\sigma_k} + \nu \right) \frac{\partial k}{\partial x_j} \right] - \varepsilon, \quad (5)$$

where k is the turbulent kinematic energy, ε is the dissipation rate of turbulent kinematic energy, and ν_t is the turbulent kinematic viscosity coefficient.

ε equation,

$$\frac{\partial \varepsilon}{\partial t} + \frac{\partial \varepsilon U_j}{\partial x_j} = -c_{\varepsilon 1} \frac{\varepsilon}{k} \overline{u_i' u_j'} \frac{\partial U_i}{\partial x_j} + \frac{\partial}{\partial x_j} \left[\left(\frac{\nu_t}{\sigma_\varepsilon} + \nu \right) \frac{\partial \varepsilon}{\partial x_j} \right] - c_{\varepsilon 2} \frac{\varepsilon^2}{k}, \quad (6)$$

where the values of the model constants are, in general, $\sigma_k = 1.0$, $\sigma_\varepsilon = 1.3$, $c_{\varepsilon 1} = 1.44$, and $c_{\varepsilon 2} = 1.92$.

The constitutive law of the nonlinear second-order k - ε model is given as

$$\begin{aligned} -\overline{u_i' u_j'} = & \nu_t S_{ij} - \frac{2}{3} k \delta_{ij} - \frac{k}{\varepsilon} \nu_t \left[\alpha_1 (S_{il} \Omega_{lj} + S_{jl} \Omega_{li}) \right. \\ & \left. + \alpha_2 \left(S_{il} S_{lj} - \frac{1}{3} S_{km} S_{mk} \delta_{ij} \right) + \alpha_3 \left(\Omega_{il} \Omega_{lj} - \frac{1}{3} \Omega_{km} \Omega_{mk} \delta_{ij} \right) \right], \end{aligned} \quad (7)$$

$$\nu_t = c_\mu \frac{k^2}{\varepsilon}, \quad (8)$$

$$c_\mu = \frac{c_{\mu 0} (1 + c_{ns} S^2 + c_{n\Omega} \Omega^2)}{1 + c_{ds} S^2 + c_{d\Omega} \Omega^2 + c_{ds\Omega} S\Omega + c_{ds1} S^4 + c_{d\Omega 1} \Omega^4 + c_{ds\Omega 1} S^2 \Omega^2}, \quad (9)$$

$$\alpha_1 = -0.1325 f_M(M), \quad (10)$$

$$\alpha_2 = 0.0675 f_M(M),$$

$$\alpha_3 = -0.0675 f_M(M),$$

$$f_M(M) = \frac{1}{1 + 0.01 M^2}, \quad (11)$$

$$M = \max(S, \Omega), \quad (12)$$

$$S = \frac{k}{\varepsilon} \sqrt{\frac{1}{2} S_{ij} S_{ij}}, \quad \Omega = \frac{k}{\varepsilon} \sqrt{\frac{1}{2} \Omega_{ij} \Omega_{ij}}, \quad (13)$$

$$S_{ij} = \frac{\partial U_i}{\partial x_j} + \frac{\partial U_j}{\partial x_i}, \quad \Omega_{ij} = \frac{\partial U_i}{\partial x_j} - \frac{\partial U_j}{\partial x_i}, \quad (14)$$

where S_{ij} and Ω_{ij} are the strain tensor and the rotation tensor, respectively. δ_{ij} is the Kronecker symbol. $c_{\mu 0}$, c_{ns} , $c_{n\Omega}$, c_{ds} , $c_{d\Omega}$, $c_{ds\Omega}$, c_{ds1} , $c_{d\Omega 1}$, and $c_{ds\Omega 1}$ are the model constants.²³

B. Flume and vegetation configuration

The main goal of the study is a numerical model investigation, and the discussion and conclusion are based on numerical model results. The experiments are used for validating the model.¹³ The dimensions of the numerical model are as follows: the vegetation region length (L) is 2 m and the width of channel (B) is 0.31 m. The

wall roughness (w) is 0.03, and the bed roughness (n) is 0.02. The model assumes a fixed bed configuration. The slope (S) of the channel is set to 1/300. The flow rate (Q) is 50 m³/h, and the downstream water depth (H) is 0.255 m.

In this study, rigid vegetation was used. The height (h) of the canopy is 0.15 m, and the canopy density $a = nd = 5.56$, 2.78, and 1.39 m⁻¹, equivalent to the number of plants per unit area (n) in the experiment is 1111, 556, and 278 m⁻² under the vegetation diameter $d = 0.5$ cm, respectively. All arrangement forms are uniform arrangement.

Vegetation growth is not limited to the vertical direction alone, it also extends horizontally, thus variations in width should also be taken into account.²⁴ Green^{25,26} provided experimental support for three vegetation blockage factors. The researcher determined blockage factors for up to nine cross sections at each station and developed an empirical model for calculating flow resistance in channels with submerged vegetation. Here, we only consider a series of effects resulting from the lateral expansion of canopies. We introduce the concept of blocking ratio (B_r), defined as the ratio of the width of the vegetation region (b) on the cross section of the water channel to the width of the water channel (B). White and Nepf²⁷ conducted experiments in a flume with vegetation arranged in a staggered equilateral pattern with 1/3 blocking ratio to assess the shear flow dynamics in the presence of a porous layer. Ben Meftah *et al.*²⁸ conducted flume experiments with a blocking ratio of 3/4 to better understand the interaction between flow behavior and canopy structure. Additionally, Yan *et al.*²⁹ used a flume with a blocking ratio ranging from 1/3 to 1/2 to study the variations in velocity profiles between vegetated and non-vegetated areas at different longitudinal adjustment distances. Therefore, The blocking ratio $B_r = 0.1, 0.25, 0.35, 0.5, 0.65, 0.75, 0.9$, and 1.0 in this study. A blocking ratio of 1.0 indicates that the water channel is completely covered by vegetation.

The average drag coefficient of vegetation is denoted as C_d . In previous studies, numerous experts and scholars have conducted in-depth research on C_d . However, estimating C_d is often challenging and can depend on various factors such as canopy density, Reynolds number, individual vegetation morphology, and so forth.^{30,31} Raupach *et al.*³² suggested that experimental evaluations should be utilized to assess C_d . With the efforts of follow-up researchers, there are more new understandings of C_d . Yan *et al.*³³ conducted experiments using a flume with submerged vegetation and suggested the drag coefficient C_d of 1.2 for the current vegetation conditions. They obtained good experimental results using this C_d value. Luhar *et al.*³⁴ summarized the experimental results of Green,²⁵ suggested that under the conditions of $a = 0.1$ cm⁻¹ and a canopy height $h = 10$ –50 cm⁻¹, a drag coefficient C_d value of approximately 1.0 is reasonable. Chen *et al.*³⁵ investigated the wake characteristics of individual cylinders with different shapes. They found C_d ranged from 1.2 to 4.5 for these shapes. Calvani *et al.*³⁶ investigated the stability of uniform flow on a non-erodible river bed using a drag coefficient C_d value of 2.0. Shi *et al.*¹⁹ carried out a narrow open channel experiment with submerged vegetation using $C_d = 1.4$. Finally, we believe that the influence of vegetation on flow structure is beneficial for the progress of current research when $C_d = 1.5$. After entering a vegetation region, the flow requires a certain distance to adjust the drag forces exerted by the vegetation and reach a momentum balance.³⁴ The threshold distance for this adjustment is typically smaller than $L_c = (C_d a)^{-1}$, also known as the drag length scale. In this study, the drag length scale $L_c = 0.12, 0.24$, and 0.48 m.

In experimental studies involving vegetation flow, solid cylinders are widely used to construct canopy models due to their simplicity and ease of measurement (see Fig. 2). This model has been used to explore the flow velocity and wake vortex structure and its effect on the deposition process.^{35,37} Based on this vegetation model, Yan *et al.*³³ used the improved Spalart–Allmaras turbulence model to study the coherent vortex. In order to facilitate the description of the spatial location of different characteristics in the channel clearly and concisely, the spatial variation of vegetation in the transverse direction using the four zones defined in Yan *et al.*³³ for the flume cross section (see Fig. 3).

We impose periodic boundary conditions at the inlet and outlet of the model domain. After performing a grid independence analysis (see Appendix), we selected a mesh of $21 \times 41 \times 35$ nodes (27 000 grid cells). To ensure the adequate development and stability of the flow, the numerical model selects the flow direction measurement location at $0.8L$, which is close to the experimental position of $0.832L$.¹³ According to the physical interpretation of the drag length scale $(C_{da})^{-1}$, it is reasonable to investigate the structure of coherent vortices at this location.³⁴ Four longitudinal velocity measuring points were placed in the middle of the vegetation region, the boundary of the vegetation region, the middle of the non-vegetation region, and the boundary of the non-vegetation region. The upstream inflow rate is maintained at a constant value of $Q = 50 \text{ m}^3/\text{h}$ and the downstream water depth, $H = 0.255 \text{ m}$. Consequently, the flow structure determines the cross-sectional average velocity $U_m = Q/(BH) = 0.176 \text{ m}^3/\text{s}$. The vegetation submergence ratio is maintained at a constant value of $H/h = 1.7$. The frontal area index, $\lambda_f = ah$, can be naturally obtained.³⁸

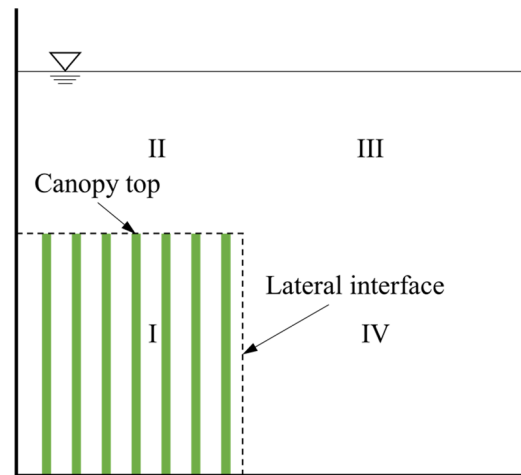


FIG. 3. Partially obstructed channel cross section partition.

Reynolds number is used to indicate the fluid motion state. White and Nepf²⁷ defined the array Reynolds number $Re_d = U_1 d/\nu$ and the open channel Reynolds number $Re_h = U_2 d/\nu$, where the U_1 and U_2 are the mean velocities in the vegetation and the open channel, to describe the significance of viscous stresses. In this study, the canopy height Reynolds number $Re_h = U_h h/\nu$ is used to represent the flow state at that location, where U_h is the average velocity at the canopy top. A series of parameters related to the research are listed in Table I.

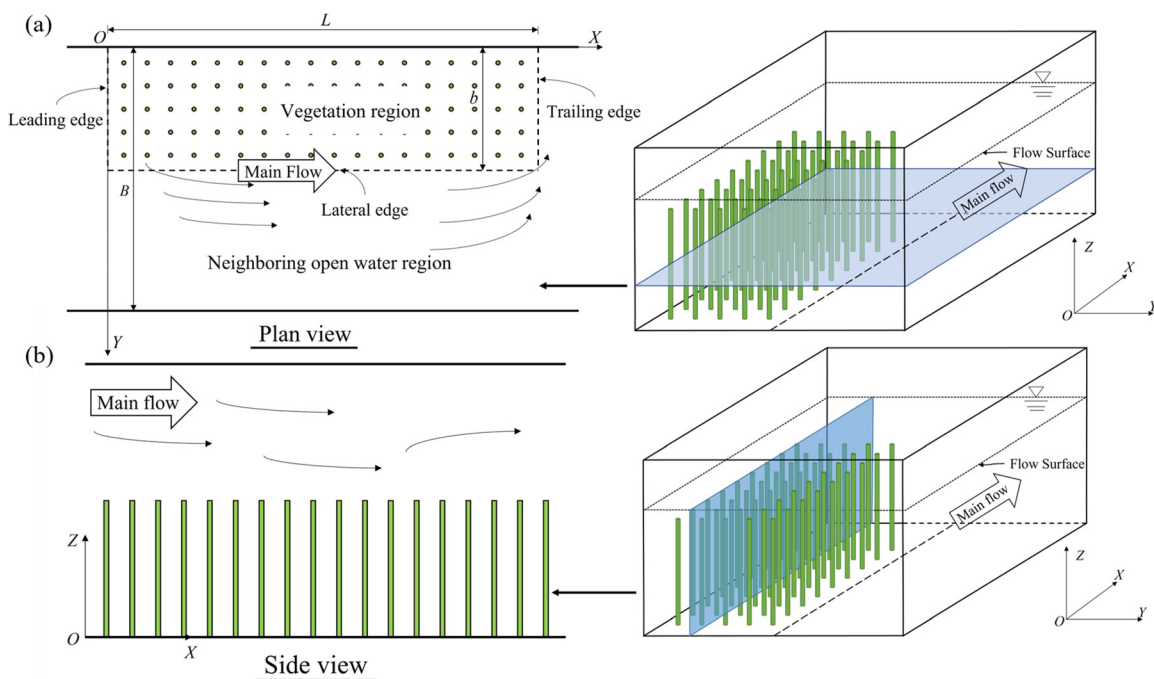


FIG. 2. Two-dimensional flow structure in (a) a partially obstructed channel with a submerged canopy, plan view and (b) side view.

TABLE I. Summary of numerical simulation runs.

Run	Q (m ³ /h)	H (m)	U_0 (m/s)	Re_h	N (m ⁻²)	a (m ⁻¹)	B_r	H/h	$(C_d a)^{-1}$
L1	50	0.255	0.176	13 109	1111	5.56	0.1	1.7	0.12
L2	50	0.255	0.176	18 232	1111	5.56	0.25	1.7	0.12
L3	50	0.255	0.176	19 426	1111	5.56	0.35	1.7	0.12
L4	50	0.255	0.176	21 473	1111	5.56	0.5	1.7	0.12
L5	50	0.255	0.176	24 046	1111	5.56	0.65	1.7	0.12
L6	50	0.255	0.176	25 363	1111	5.56	0.75	1.7	0.12
L7	50	0.255	0.176	26 524	1111	5.56	0.9	1.7	0.12
L8	50	0.255	0.176	25 387	1111	5.56	1.0	1.7	0.12
M1	50	0.255	0.176	16 216	555	2.78	0.1	1.7	0.24
M2	50	0.255	0.176	18 718	555	2.78	0.25	1.7	0.24
M3	50	0.255	0.176	20 334	555	2.78	0.35	1.7	0.24
M4	50	0.255	0.176	23 513	555	2.78	0.5	1.7	0.24
M5	50	0.255	0.176	25 410	555	2.78	0.65	1.7	0.24
M6	50	0.255	0.176	26 431	555	2.78	0.75	1.7	0.24
M7	50	0.255	0.176	27 260	555	2.78	0.9	1.7	0.24
M8	50	0.255	0.176	25 222	555	2.78	1.0	1.7	0.24
S1	50	0.255	0.176	17 090	278	1.39	0.1	1.7	0.48
S2	50	0.255	0.176	19 618	278	1.39	0.25	1.7	0.48
S3	50	0.255	0.176	21 930	278	1.39	0.35	1.7	0.48
S4	50	0.255	0.176	25 016	278	1.39	0.5	1.7	0.48
S5	50	0.255	0.176	26 532	278	1.39	0.65	1.7	0.48
S6	50	0.255	0.176	27 348	278	1.39	0.75	1.7	0.48
S7	50	0.255	0.176	27 593	278	1.39	0.9	1.7	0.48
S8	50	0.255	0.176	24 830	278	1.39	1.0	1.7	0.48

III. RESULT

A. Numerical model validation

In order to validate the present numerical model setup, we reproduced one case (run L1) of the experiments presented in Yan *et al.*¹³ Figure 4 shows the comparison between the numerical simulations (solid lines) and the experimental measurements (markers) in terms of vertical distribution of the longitudinal velocity. The performance of the numerical model is fairly satisfactory. In fact, the majority of the experimental data fall in the colored shaded band that represents the $\pm 20\%$ error. The mean squared error (MSE) = 0.0036–0.0123 and the root mean squared error ($RMSE$) = 0.0604–0.1107, both demonstrating acceptable levels of error. Specifically, the simulation results for the velocity in the middle of the non-vegetation region [see Fig. 4(d)] exhibit the smallest errors (MSE = 0.0036 and $RMSE$ = 0.0604). It is worth noting that the good agreement between the numerical predictions and the experiments, especially in the vegetated region (MSE = 0.0049 and $RMSE$ = 0.0699), suggests that the numerical model can capture the turbulent characteristics of the flow.

B. Longitudinal flow velocity and turbulent kinetic energy

In this section, we show the results in terms of the distribution of longitudinal velocity and turbulent kinetic energy under different vegetation densities and coverage levels. Examples of vertical profiles of the

non-dimensional longitudinal velocity for different values of B_r are shown in Fig. 5. The profiles are extracted from different locations within the domain, in particular, within the vegetation [Figs. 5(a)–5(c)] and in the non-vegetated region [Figs. 5(d)–5(f)]. The typical S-shaped profiles inside the vegetated area are recovered consistently with previous experimental studies.^{32,39,40} Moreover, the presence of an inflection point at the top of the canopies, i.e., for $z^* = 1$, is observed and follows the experimental findings reported by White and Nepf²⁷ and Nepf *et al.*¹⁶ This inflection point plays a significant role in promoting the growth of Kelvin–Helmholtz vortices, as noted by Rominger and Nepf.²⁴ The lateral expansion of canopies compresses the space in the non-vegetation region, thereby affecting the distribution pattern of the velocity in the middle. See the profiles shown in Fig. 5 panels. When $B_r = 0.1$ and 0.25, the velocity distribution conforms to the logarithmic distribution form, but with the increase in B_r value, the S-shaped distribution of longitudinal velocity becomes more obvious. This phenomenon may be attributed to the influence of coherent vortices generated by the lateral expansion of vegetation.

From Fig. 6, it can be observed that for a lower blocking ratio ($B_r = 0.1$), zone I exhibits a lower velocity, while the higher velocity is mainly concentrated in zones II and III. When $B_r = 0.25$ –0.75, the higher velocity regions “intrude” into zone IV, leaving only zone I with a noticeable lower velocity. In the study by Choi and Kang,¹⁷ this intrusion phenomenon was also observed. Finally, at a higher blocking ratio $B_r = 0.9$ –1.0, zone IV is influenced by the presence of the wall

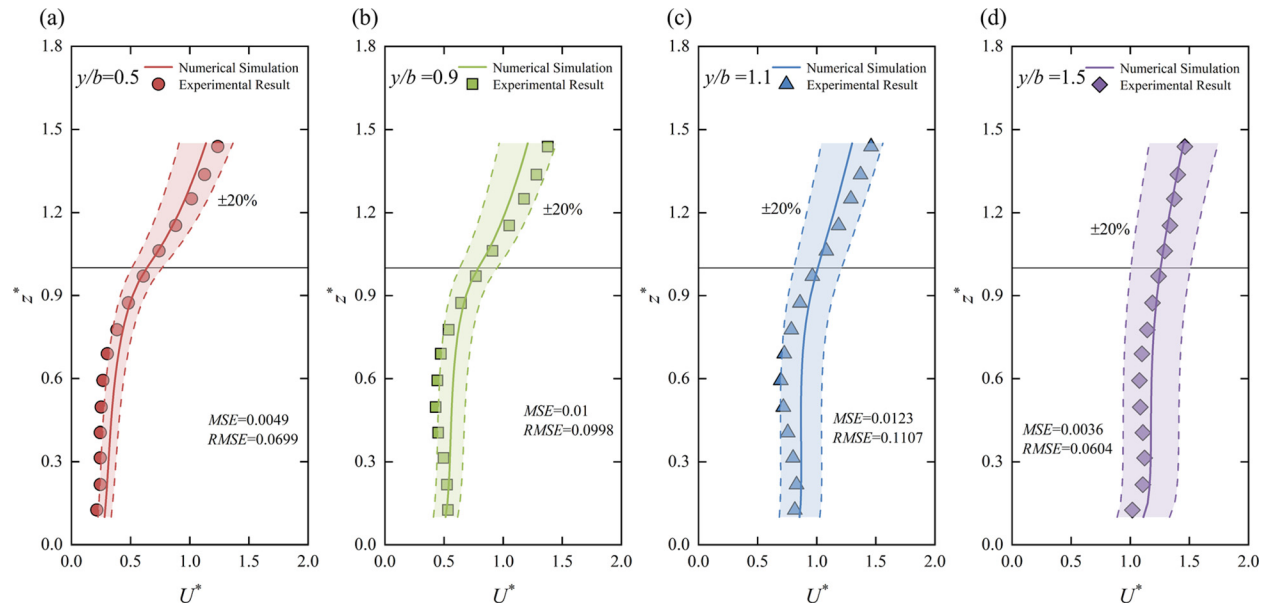


FIG. 4. Comparison of the vertical profile of the longitudinal velocity between the numerical simulations (solid lines) and the experimental observations (markers). $z^* = z/h$, normalized with canopy height. $U^* = U/U_m$, normalized with cross-sectional mean velocity (U_m). The horizontal fine line is the canopy top. (a)–(d) are different measurement positions, respectively.

and the lateral boundaries of the vegetation region. As a result, the higher velocity regions shift upward to zones II and III. For the runs M and S scenarios, a decrease in canopy density results in a weaker intrusion phenomenon, and the distribution of flow velocities in the cross section tends to be relatively uniform. It can be easily observed that the blocking ratio affects the velocity distribution pattern of the section, while the vegetation density indirectly controls the velocity of the whole section by directly controlling the velocity in the vegetation area.

We consider the regions (II and III) not directly affected by the lateral expansion of vegetation as zone A, while the regions (I and IV) directly influenced by it are considered as zone B. We quantify the influence of vegetation lateral expansion on the cross-sectional velocity using the discharge ratio (Q_r) between the two zones. This method is expressed by the following equation:

$$Q_r = \frac{Q_A}{Q_B} = \frac{\overline{U_A} S_A}{\overline{U_B} S_B}. \quad (15)$$

As shown in Figs. 7(a)–7(c), both canopy density and blocking ratio result in variations in the discharge ratio (Q_r). We use the exponential function to fit, and get an excellent fitting result ($R^2 = 0.96$ – 0.97). Under a low blocking ratio ($B_r < 0.5$), the relationship between Q_r and B_r shows lower sensitivity to changes in canopy density, and velocity changes tend to be within the layer (see Fig. 7). When the channel exceeds the half-blockage state, the stratification phenomenon is gradually affected by changes in canopy density, and velocity changes tend to be interlayer changes.

Turbulent kinetic energy (k) is the energy of vortex motion in turbulent flow. Due to the influence of canopy density and blocking ratio, k exhibits significant temporal and spatial variations. As shown in Fig. 8, k exhibits a distribution pattern that radiates from a central

point to its surroundings. This central point (k global maximum point) is attributed to the coexistence of three-dimensional coherent vortices (vertical and lateral).¹³ When $B_r = 0.1$ – 0.5 , the center point is located near the canopy lateral edge. However, when $B_r = 0.65$ – 1.0 , the center point shifts toward the canopy top. It appears that canopy density primarily influences the magnitude of k , but it does not have a significant impact on the distribution pattern. Compared with the lateral edge of the vegetation region, the increase in the blocking ratio has a more obvious effect on k at the canopy top. This phenomenon should be due to the increase in the blocking ratio, which leads to the increase in the contact area between the canopy top and the water flow, resulting in a larger k . We can find some support in the phenomenon that the k of the lateral edge of the vegetation region does not change significantly with the blocking ratio (the contact area between the lateral edge and the water flow does not change).

C. Turbulence anisotropy characteristics

We commonly use Reynolds stresses to represent turbulence anisotropy. Herein, we analyze and evaluate turbulence anisotropy by taking the difference between the vertical and lateral components of Reynolds stresses.¹³ As shown in Fig. 9, at the top and lateral edge of the canopy, two different Reynolds stresses dominate and form two circular distribution patterns with a central peak that attenuates toward the periphery. This phenomenon is consistent with the observations made by Yan *et al.*¹³ In different runs, the larger canopy density leads to a more obvious expression of turbulence anisotropy, but there is no difference in the distribution pattern. As shown in Fig. 8, the distribution pattern of kinetic turbulent energy directly reflects the characteristics of turbulence anisotropy. Due to the coevolution of vertical and lateral coherent vortices, turbulence anisotropy becomes a significant factor influencing the turbulent field in partially obstructed

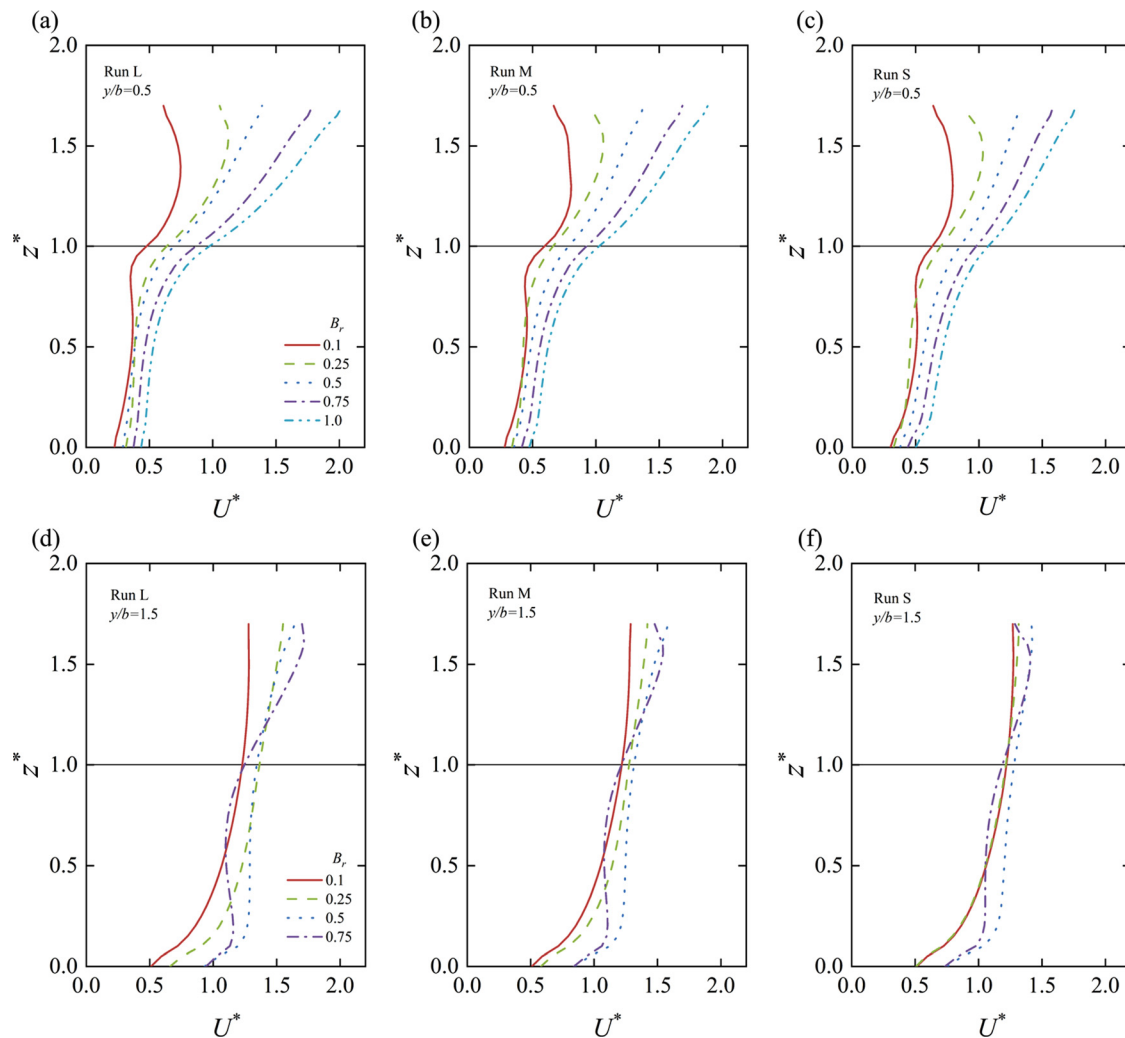


FIG. 5. The velocity distribution in the middle of (a)–(c) the vegetation region ($y/b = 0.5$) and (d)–(f) non-vegetation region ($y/b = 1.5$) under run L, M, and S, respectively.

channels with submerged vegetation.¹³ The present results suggest that the blocking effect of the canopy induces a strong anisotropy of the Reynolds stresses and, ultimately, triggers the generation of macrovortices able to modify the momentum exchange at the interface between the vegetated and non-vegetated regions.

Jia *et al.*¹⁰ investigated the temporal variation of Reynolds stresses at the canopy lateral edge. On the contrary, we mostly focus our attention on the spatial variation. When the canopy expands laterally, increasing the blocking ratio, it is evident that the Reynolds stress at the canopy top exhibits a stronger effect. As for the Reynolds stress at the canopy lateral edge, its influence undergoes a process of initially increasing and then decreasing in strength. Similar to the study by Yan *et al.*,¹³ the influence of Reynolds stress at the boundary of the vegetation area also leads to significant momentum exchange in the mixing flow process, and the maximum momentum flux always overlaps with the canopy lateral edge. Mixing flow also generates canopy-scale coherent vortices that develop along the flow direction at the canopy lateral edge.¹⁰

Combining Figs. 8 and 9, we observe a close correlation between the anisotropic characteristics of turbulence and its kinetic energy. However, further studies are needed to establish the intrinsic relationship between anisotropic characteristics and turbulent kinetic energy. At least for low ($B_r = 0.1$) and high blocking ratios ($B_r = 1.0$), the distribution patterns of both parameters are similar.

IV. DISCUSSION

A. Evolution characteristics of secondary flows

Vegetation exerts a noticeable resistance on water flow, leading to the generation of secondary circulation. Nezu and Onitsuka⁴¹ suggested that the presence of vegetation in a flow field leads to the generation of time-averaged secondary flows due to the anisotropy of turbulence. The blocking ratio plays a crucial role in controlling the variation of the cross-sectional secondary flows. Ghisalberti and Nepf⁴² suggested that the flow above the mixing layer is likely influenced by the presence of secondary flows, making it challenging to

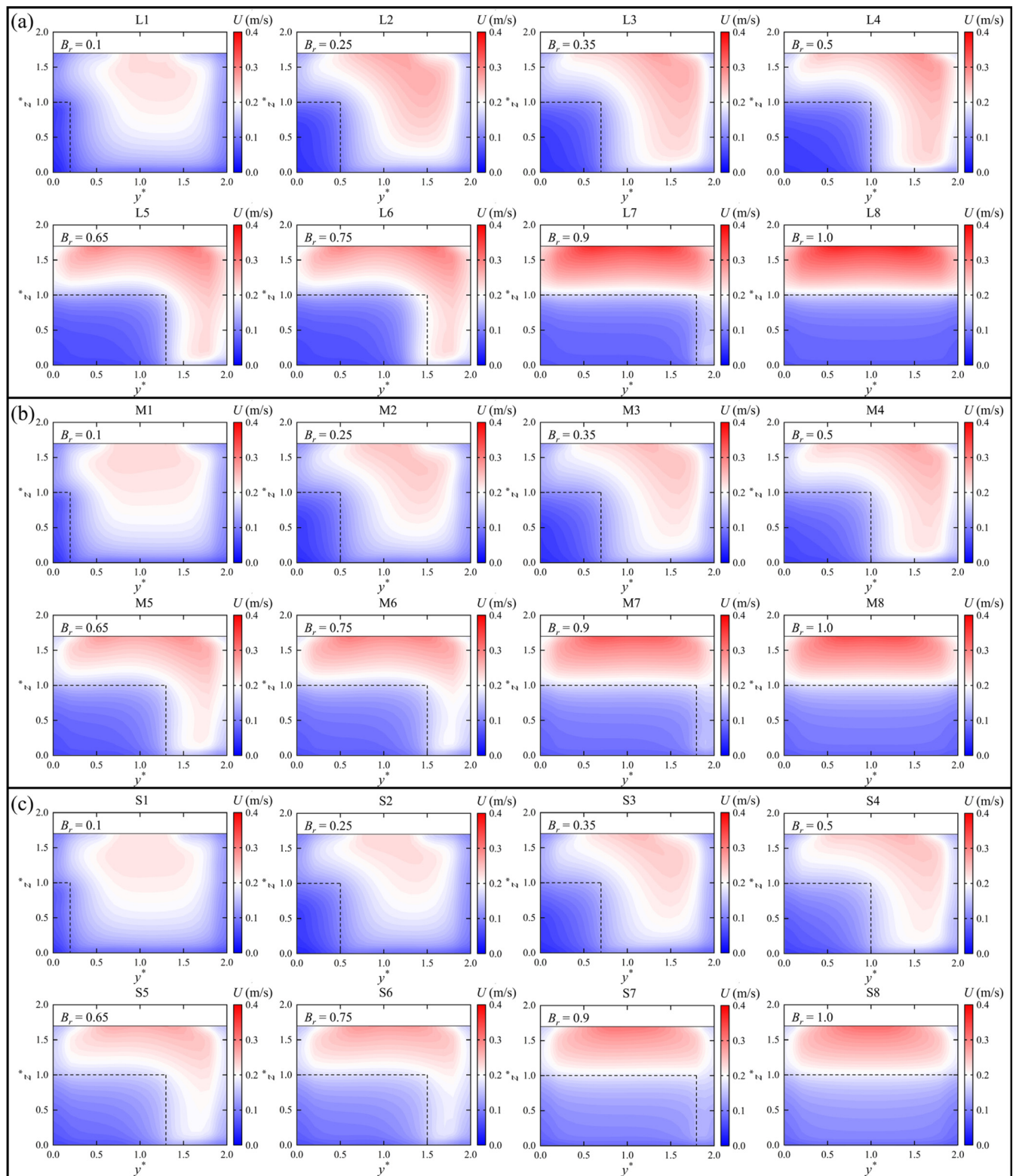


FIG. 6. Spatial patterns of longitudinal velocity for all runs in Table I. (a)–(c) are runs L, M, and S, respectively. U is the longitudinal velocity (m/s).

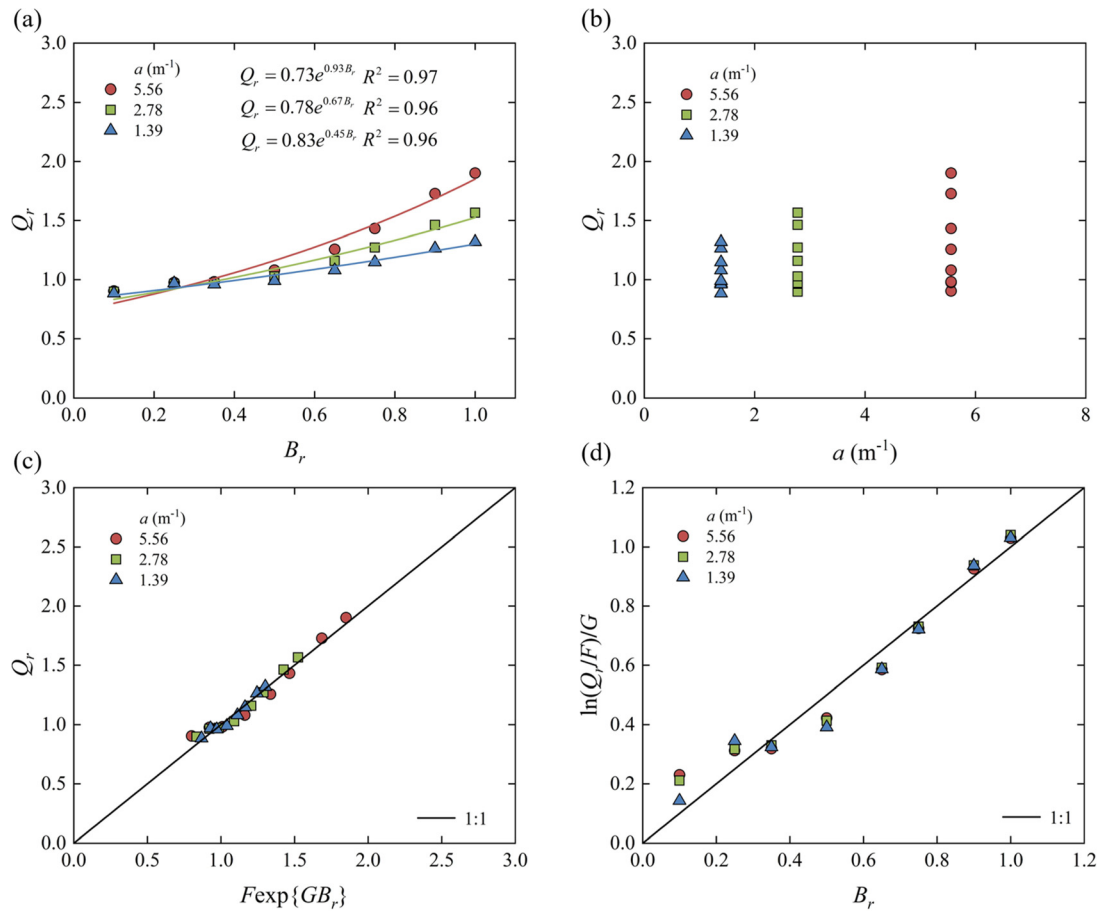


FIG. 7. Variation of discharge ratio of canopy with different canopy density during lateral expansion. The relationship between (a) blocking ratio and flow ratio, (b) canopy density and flow ratio, and (c) and (d) are the relationships between the predicted and actual value.

describe using a simple one-dimensional flow momentum equation $gS = \frac{\partial \overline{u'w'}}{\partial z} + \frac{1}{2} C_d a U^2$. Due to the strong secondary flows induced by vegetation in the upper portion of the mixing layer, a secondary flow structure can also form in the free-surface region. Yan *et al.*¹³ conducted an in-depth analysis and discussion on the sectional circulation, suggesting that the anisotropy of three-dimensional coherent vortices generates the circulation, which controls the momentum of convection.

As shown in Fig. 10, The obstruction caused by the canopy leads to the generation of secondary flows at the canopy top, like the observations made by Nezu and Sanjou.⁴³ Similarly, the secondary flows also occur at the canopy lateral edge. The secondary flows induced by the anisotropic vortex structures around the canopy, as mentioned by Yan *et al.*,¹³ align with the secondary flows observed in this study in terms of location and rotational direction. However, what differs is that the secondary circulation structures generated at the canopy top and lateral edge are more pronounced in this study.

For increasing the width of the vegetated region, the secondary flows at the canopy top exhibits both lateral motion parallel to the vegetation and a tendency to sink into the interior of the vegetated region. The scale of the secondary flows increases, and once $B_r > 0.5$, the scale

stabilizes at a relatively fixed value. Indeed, this process is easy to understand. With smaller blocking ratios, the development area for the secondary flows is limited, which prevents it from reaching a fully established scale. For the secondary flows at the vegetation lateral edge, the widening of the canopy leads to a tendency for the secondary flows to follow the boundary motion. As it approaches the opposite wall, the overall structure enters the interior of the vegetation region. The canopy density has a certain influence on the distribution of secondary flow. The secondary flow structure of run L8 is closer to the canopy top than that of S8 in the vegetation region. The larger canopy density can be used to inhibit the secondary flow structure to further invade the vegetation area as an explanation. This phenomenon is also found under other conditions of runs L and S.

Shi *et al.*¹⁹ found that on the submerged canopy lateral edge, the vertical distribution of the secondary transverse velocity exhibits three distinct sections at different heights. Our results seem to be in accordance with the latter observation. We found that when the blocking ratio $B_r = 0.35\text{--}0.75$, the vertical distribution of the secondary transverse velocity consists of three distinct sections. (1) Near the free water surface, $z^* = 1.3\text{--}1.7h$, the transverse velocity can be ignored. (2) Near the canopy top, $z^* = 0.6\text{--}1.3h$, the transverse velocity direction is

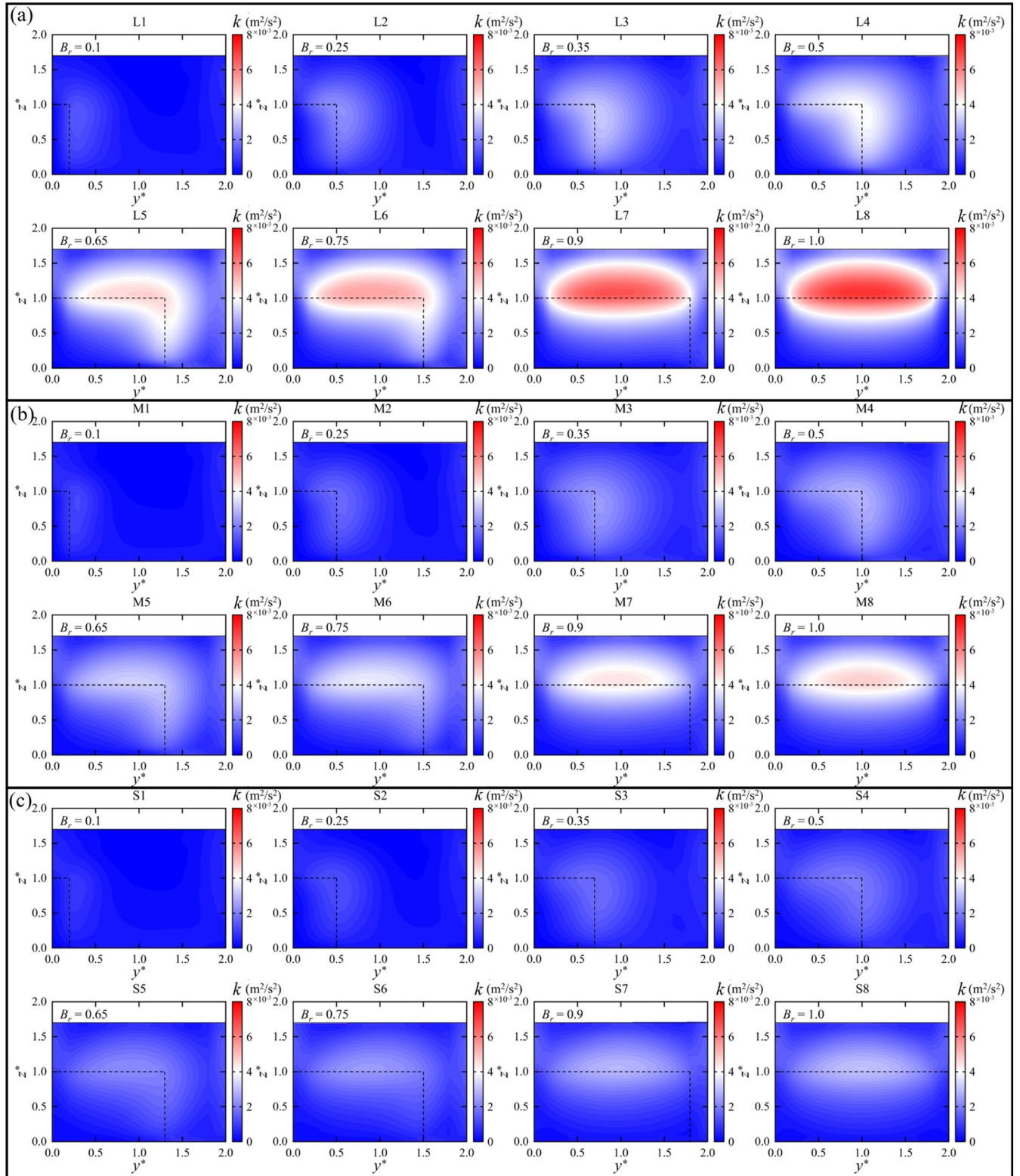


FIG. 8. Spatial patterns of kinetic turbulent energy for all runs in Table I. (a)–(c) are runs L, M, and S, respectively.

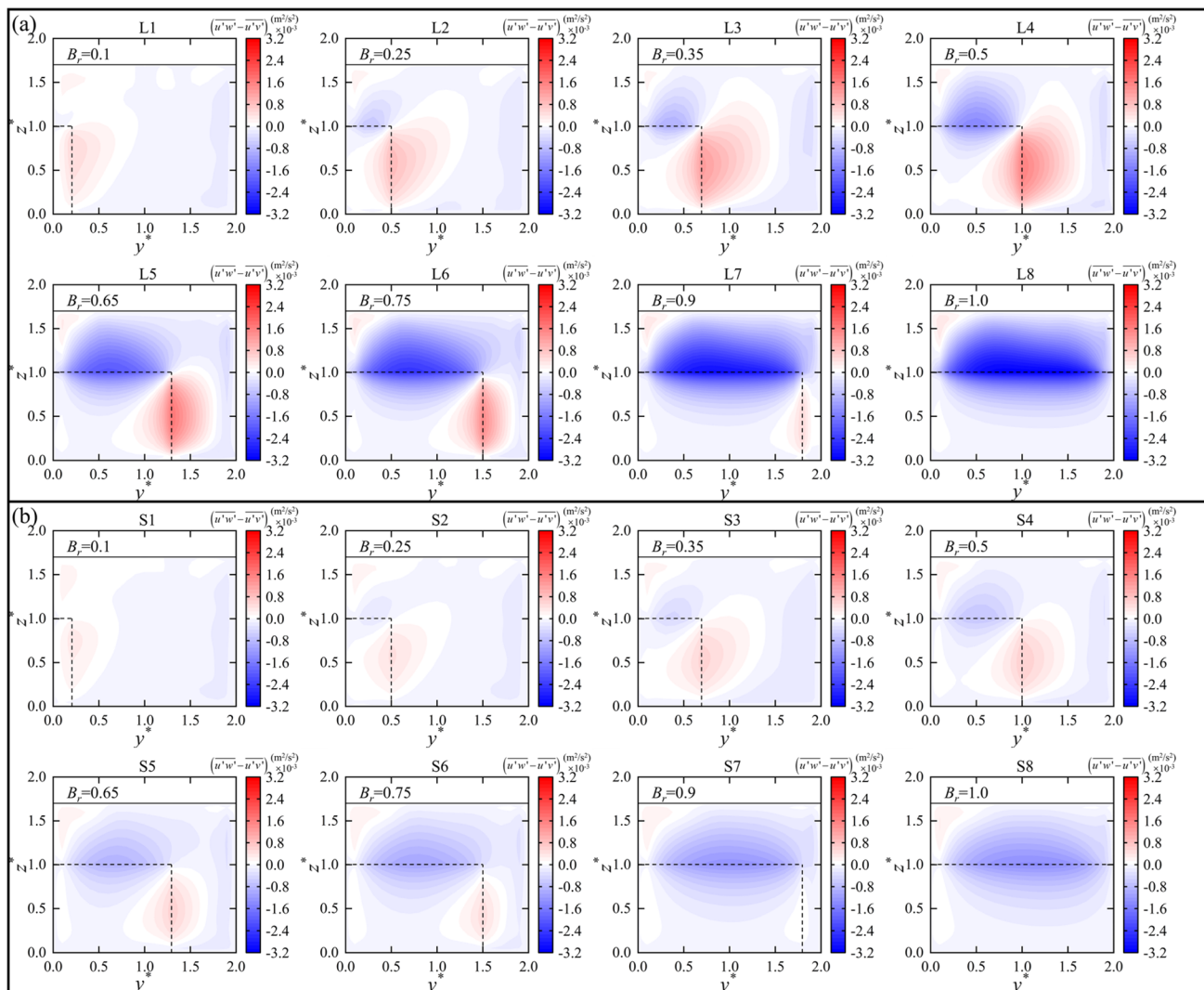


FIG. 9. Turbulence anisotropy characteristics. (a) and (b) are runs L and S, respectively.

parallel to the canopy top toward the outside of the canopy lateral edge. (3) Near the bed, $z^* < 0.6h$, the transverse velocity direction is parallel to the canopy top toward the inside of the canopy lateral edge. However, when $B_r < 0.35$ or $B_r > 0.75$, the vertical distribution of the secondary transverse velocity cannot be ignored at the free water surface. Based on our findings, two-directional secondary circulation structures occur near the two sidewalls of the free water surface. These two secondary circulations also control the secondary transverse velocity at the free water surface.

Yan *et al.*⁴⁴ obtained consistent results with the secondary flow direction near the free surface in their LES simulations of fully submerged vegetation in open channel flow, thus confirming the validity of our study. However, this phenomenon was not supported in the study by Choi and Kang⁴⁵ for flows with larger breadth–depth ratios. Therefore, the breadth–depth ratio of the channel significantly influences the distribution pattern of secondary flows. Further research is

needed to determine the specific breadth–depth ratios that cause variations in the distribution pattern of secondary flows.

As shown in Figs. 5(a), 10(a), and 10(b), the velocity dip phenomenon⁴⁶ is observed when the canopy blocking ratio is low ($B_r = 0.1$ and 0.25). In this case, the secondary flow structure near the free surface is precisely intersected by the longitudinal velocity passing through the middle part of the vegetation area. Yan *et al.*¹³ proposed that the velocity dip is induced by the formation of secondary flows arising from turbulence anisotropy.

B. Three-dimensional coherent vortex

Yan *et al.*¹³ proposed that in studies on partially obstructed channels by vegetation, the main hydraulic process involved the generation of three-dimensional coherent vortices at the canopy top and lateral edge. The author also proposed a direct method to evaluate the

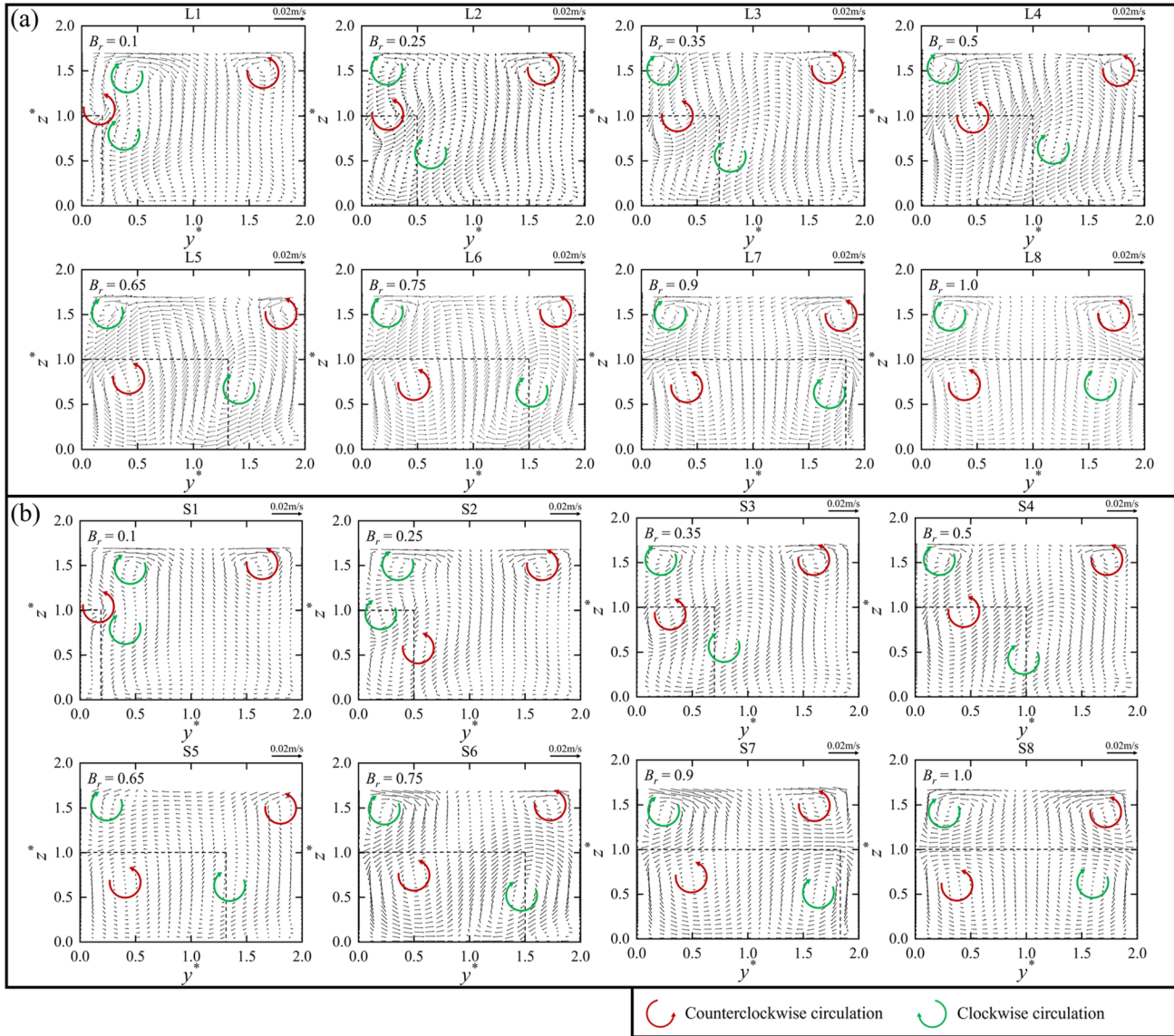


FIG. 10. The distribution of secondary flows in transverse section under transverse expansion of canopy. (a) and (b) are runs L and S, respectively.

dominance of coherent vortices by utilizing the ratio of vertical and horizontal Reynolds stresses,

$$R_{vh} = \frac{\frac{1}{b} \int_0^b -\overline{u'w'}_{\max} dy}{\frac{1}{h} \int_0^h -\overline{u'v'}_{\max} dz}. \quad (16)$$

This method of assessing the dominance of three-dimensional coherent vortices using the ratio of vertical and horizontal Reynolds

stresses is simple to calculate and easy to understand. It provides a straightforward indication of the relative importance of vertical and horizontal coherent vortices in governing the mixed flow dynamics.

When the channel is completely blocked, R_{vh} tends to infinity, indicating that it is solely dominated by the vertical Reynolds stresses at the canopy top. It is reasonable to assume that when there is no canopy blockage in the channel, R_{vh} should be zero. We assume that B_r and R_{vh} satisfy the following expressions $R_{vh} = \alpha_R e^{\beta_R/(1-B_r)}$, where α_R and β_R are undetermined coefficients. As shown in Fig. 11(a), there is a significant correlation ($R^2 = 0.982-0.997$) between the blocking ratio B_r and R_{vh} for different canopy densities. We find that α_R is a constant and β_R has a significant linear relationship [Fig. 11(b)]. Excluding the influence of canopy density, $\ln(R_{vh}/\alpha_R)/\beta_R = (1 - B_r)^{-1}$ can well

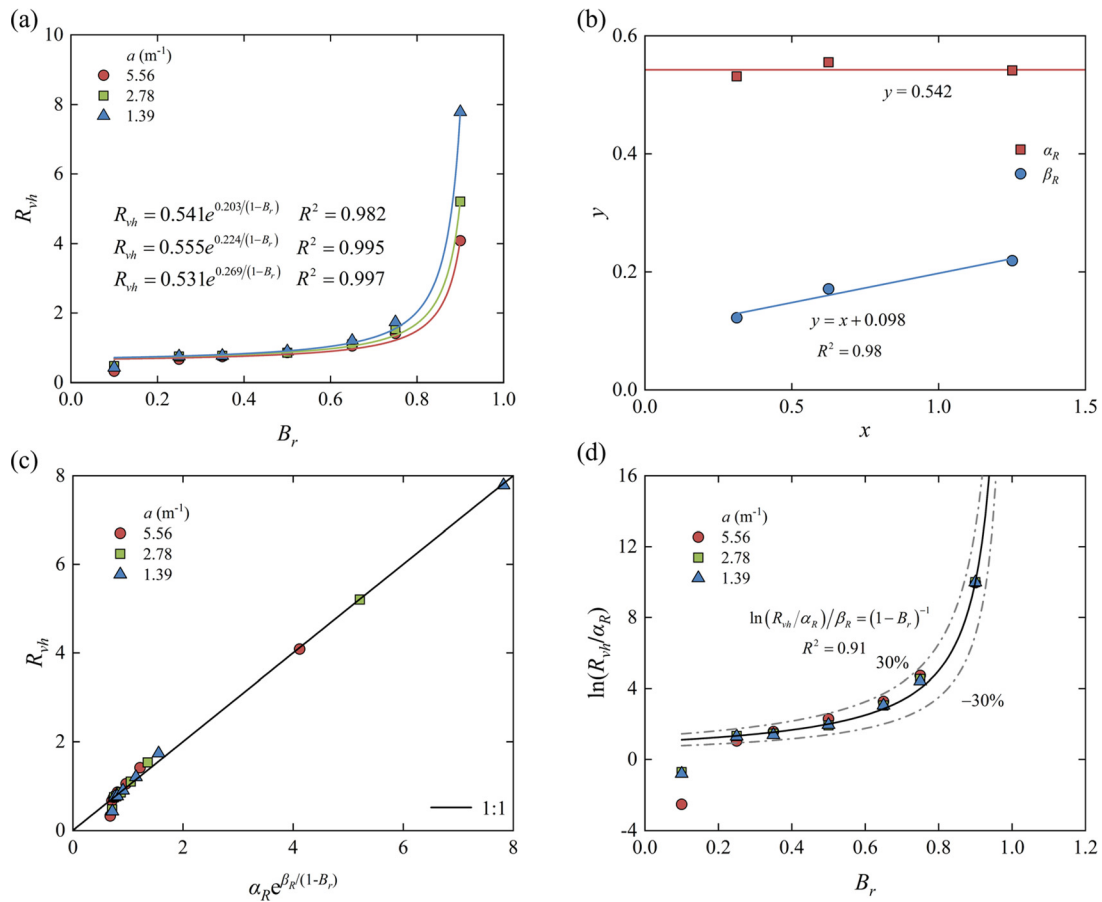


FIG. 11. Ratio of the width-averaged vertical Reynolds shear stress to horizontal Reynolds shear stress. (a) The relationship between blocking ratio and R_{vh} , (b) parameter correlation, and (c) and (d) are the relationships between the predicted and actual value.

express this relationship ($R^2 = 0.91$) [Figs. 11(c) and 11(d)]. The formation of horizontal coherent vortices has a certain spatial scale.²⁷ Therefore, an increase in the blocking ratio leads to the compression of coherent vortices, which to some extent inhibits the dominant role of horizontal coherent vortices. Instead, the vertically coherent vortices, which are less constrained in height, dominate the subsequent flow mixing process. The simulated R_{vh} at the half-blockage ($B_r = 0.5$) approximates 1 [Fig. 11(a)], which is consistent with the experimental results under similar flow configurations (see Yan *et al.*¹³) In more detail, the differences in R_{vh} resulting from changes in canopy density are not discussed in this paper. Considering only the variation in a single flow rate might introduce interference and lack meaningful discussion. Therefore, the relationship between R_{vh} and canopy density in various flow conditions, as mentioned in Yan *et al.*,¹³ remains of significant reference value.

The Reynolds number Re_h is commonly used to describe the flow conditions of fluid in the canopy top. Figure 12 depicts the relationship between the blocking ratio and the Reynolds number Re_h . Evidently, B_r and Re_h exhibit a relatively simple linear relationship, indicating a strong correlation ($R^2 = 0.80$) in the linear function.

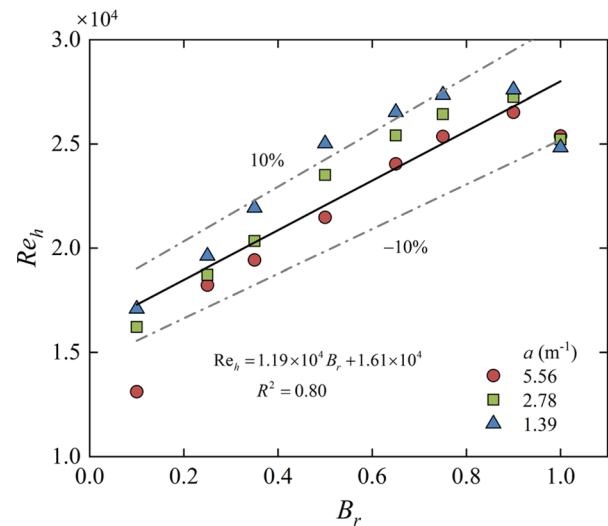


FIG. 12. The depth-related Reynolds number.

C. The structural characteristics of the mixing layer and the characteristic scale of the vertical coherent vortex

It is observed that when vegetation expands laterally, there are significant changes in the longitudinal velocity pattern in the middle of the vegetation region. These changes in velocity pattern indicate variations in the thickness of the mixing layer, t_{mb} , which lead to changes in the vertical coherent vortex penetration length.¹⁵ In general, the thickness of the mixing layer can also be represented by the momentum thickness (θ) of the mixing layer,²⁷

$$\theta = \int_0^{Z_2} \left[\frac{1}{4} - \left(\frac{U - \bar{U}}{\Delta U} \right)^2 \right] dz, \quad (17)$$

where $\Delta U = U(Z_2) - U(Z_1)$, $\bar{U} = [U(Z_2) + U(Z_1)]/2$.

As shown in Fig. 13, the momentum thickness and the process of the mixing layer increases with the increase in the blocking ratio. There is a good nonlinear fit describing this trend ($R^2 = 0.75$). When the channel reaches a state of severe obstruction ($B_r > 0.65$), the momentum thickness of the mixing layer approaches a constant value. However, in the case of lower canopy density ($a = 1.39 \text{ m}^{-1}$), there is some fluctuation in the momentum thickness. This may be attributed to the instability caused by weaker momentum exchange processes. Additionally, based on the fixed penetration length depicted in Fig. 14(a), it can be inferred that the variations in momentum thickness are primarily influenced by the evolution of outer zone vortices. Despite this, it may also be caused by low canopy density. As shown in Fig. 14, using a similar method to analyze the relationship between B_r and R_{vp} , we assume that $\delta_e = \alpha_\delta \ln(B_r) + \beta_\delta$, where α_δ and β_δ are undetermined coefficients. A favorable correlation between δ_e and B_r under the influence of the dimensionless number C_{dah} ($R^2 = 0.87 - 0.91$) is obtained. The coefficients α_δ and β_δ have a good linear correlation. Without considering the influence of C_{dah} , the correlation coefficient $R^2 = 0.89$.

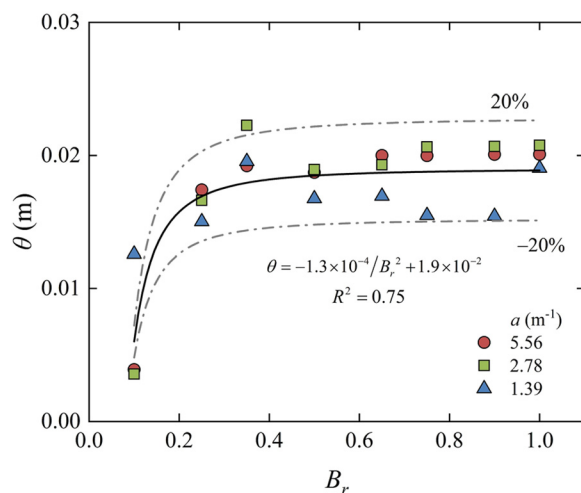


FIG. 13. The momentum thickness of the mixing layer under the influence of blocking ratio (B_r).

In the study conducted by White and Nepf²⁷ on the growth of the shear layer downstream of a baffle, it was observed that the momentum thickness reached a relatively stable value after a certain distance of development. In the study, the significant changes in momentum thickness occur during the development stage of the vortices. Subsequently, with the vortex-induced entrainment of the surrounding fluid, the vortices are influenced by momentum over larger distances, leading to the growth of the mixing layer. Moltchanov *et al.*⁴⁷ suggested that the complete development of the mixing layer occurs at a position $x = 9L_c - 13L_c$ behind the leading lateral edge of the vegetation region. Therefore, based on existing knowledge, this paper puts forward a hypothesis. Although vegetation obstruction can generate vertical coherent vortices, too low a blocking ratio leads to the vortices being located too close to the wall. In this case, similar to the near-bed momentum exchange process dominated by bed friction effects mentioned in Yan *et al.*,¹³ the wall friction effect governs the momentum exchange near the wall. As a result, the mechanism of momentum thickness generation differs in this region compared to areas with a higher blocking ratio.

Due to the significant difference in momentum thickness when $B_r = 0.1, 0.25$, and 0.35 , and the relatively minor impact of blocking ratio variation on momentum thickness when $B_r = 0.5$ and 0.65 , the drastic changes in momentum thickness are more likely to be attributed to the influence of sidewall friction effects, which are comparable to bed friction effects. Nevertheless, further experimental investigations are needed to validate this speculation. It is also a promising direction to explore the influence of vertical coherent vortices on momentum exchange processes in the context of lateral expansion of the canopy.

After undergoing sufficient development, coherent vortices typically exhibit noticeable periodicity in space. Meanwhile, the momentum exchange reaches a relatively stable state. Furthermore, the vortex size tends to be stable.^{15,38} Wang *et al.*⁴⁸ used DA-LES (depth-averaged large-eddy simulation) to simulate the evolutionary characteristics of the inner and outer vortex scales in the partially distributed canopy flows, and found that the inner and outer vortices were controlled by canopy density and other factors, and the development of the vortex scales was highly asymmetric. Jia *et al.*¹⁰ found that the growth period of the inner region scale (δ_i) of the coherent vortices is very short. Even though the outer region vortices continue to evolve, the inner region scale is not significantly affected. The fundamental reason for this is the resistance caused by the penetration force of the canopy on the vortices. Moreover, in the absence of sidewall effects, the inner region scale is only influenced by the drag length scale.⁴⁹ Indeed, this result provides further evidence to support the earlier assertion that the evolution of outer region vortices leads to changes in momentum thickness.

Compared to rigid emergent vegetation, submerged vegetation in the form of a roughness layer exhibits discontinuities in depth. The flow structure becomes three-dimensional. These differences in conditions introduce vertical high-momentum exchange processes that are absent in the case of rigid emergent vegetation. As shown in Fig. 14(a), there is no significant change in the penetration length after partial vegetation blockage. At this point, the scale is determined by the drag length scale, L_c . Overall, it reflects the inhibitory effect of high density and resulting high resistance on the vortex penetration. Under three canopy densities ($a = 5.56, 2.78$, and 1.39 m^{-1}), the vertical coherent vortex penetration length $\delta_i \approx 2.5\theta, 2.8\theta$, and 3.3θ , respectively. The

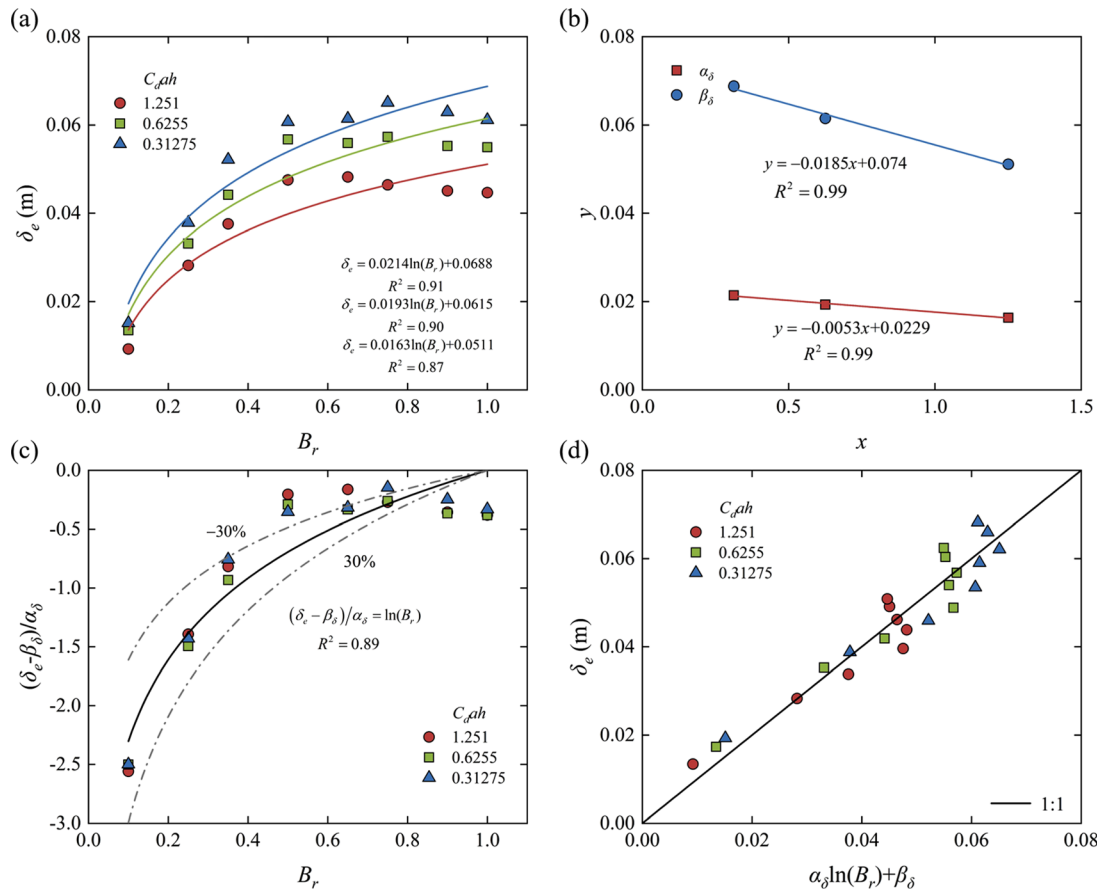


FIG. 14. The vertical coherent vortex penetration length. (a) The relationship between B_r and δ_e , (b) parameter correlation, and (c) and (d) are the relationships between the actual δ_e and the predicted value of the fitted equation.

vertical dimension $\delta_v \approx (6.3-7.0)\theta$, $(6.6-7.4)\theta$, and $(7.2-9.0)\theta$, respectively. Ghisalberti and Nepf¹⁵ demonstrated that for flexible vegetation, when the mixing layer thickness reaches its maximum value, $\delta_v \approx 6\theta$. For rigid vegetation, an approximation using the mixing layer thickness resulted in $\delta_v \approx (6.4-7.8)\theta$. The present results are consistent with previous studies. Indeed, we can discuss the reasons behind the difference in vertical dimensions of vortices generated by rigid and flexible vegetation. One reason is that flexible vegetation, due to the occurrence of the “monami” phenomenon,⁵⁰ results in canopy geometries that are not always favorable for the presence of current vortices. However, vortices can always encounter the fixed drag geometry responsible for their formation in rigid canopies.⁵¹ Additionally, rigid vegetation exhibits a faster momentum exchange process. Therefore, the vertical coherent vortices in flexible vegetation are smaller at the same mixing layer scale. As for the vortex penetration length of vortices, which is of greater interest to us, flexible vegetation is not highly sensitive to canopy curvature.³⁸ Consequently, we primarily focus on the vertical coherent vortex penetration length in rigid vegetation.

We found that the vertical coherent vortex penetration scale is jointly controlled by C_dah and B_r (see Fig. 14). Of course, other factors cannot be ruled out, but the following equation can still be used to describe the penetration scale controlled by the above two variables:

$$\delta_e = (0.055 \pm 0.0028)(C_dah)^{(0.21 \pm 0.053)} B_r^{(0.42 \pm 0.057)} (\delta_e \leq h). \quad (18)$$

The fitting result with $R^2 = 0.83$. The notion is that the blocking ratio and drag length scale have a significant impact on the vertical coherent vortex penetration length. We found that although the change in the blocking ratio has a stronger influence on the penetration scale of the vertical coherent vortex, B_r can only be valued between 0 and 1, and canopy density has more flexibility in this regard. Although the variation of vertical frontal area is not addressed in this study, in natural environments, C_d does not maintain a constant value in the vertical direction, and the variation of C_d with vertical frontal area significantly affects the structure of the flow,^{52,53} which in turn alters the penetration scale of the vertical coherent vortex. Equation (18) does not apply to the above case, but the authors believe that Eq. (18) is still formally intuitive, even when the condition of C_d variation is taken into account. This requires further subsequent verification.

V. CONCLUSION

Vegetation growing in river channels is usually not static, as its growth and proliferation are accompanied by changes in flow structures. Many studies have focused on cases where the width of the

vegetation region remains constant. However, the lateral expansion of canopies significantly affects the structure of cross-sectional secondary flows and the development of three-dimensional coherent vortices. Therefore, relying solely on existing research is insufficient to fully uncover the range of impacts vegetation has on water flow structures. To fill this gap, this study aims to investigate a series of variations in flow structures when vegetation expands laterally. Additionally, the study will incorporate the effects of canopy density changes and comprehensively consider the influence of channel blockage on flow structures. By varying the canopy density and blocking ratio, this study has designed 24 different runs, encompassing a wide range of situations.

Significant secondary flows and lateral velocities are generated at the canopy top and lateral edge. Changes in the blocking ratio strongly influence the behavior of secondary flows. At the vegetation region edges, the secondary flows exhibit three different forms of lateral velocities near the free surface, canopy top, and bed. In the fully submerged canopy channel near the free surface, it was observed that the distribution pattern of secondary flows is influenced by the breadth–depth ratio of the channel.

Three-dimensional coherent vortices are influenced by vertical and transverse Reynolds stresses. We have observed an exchange in the dominant role of the two Reynolds stresses during the lateral expansion of canopies. This change trend can be reasonably described by an equation with a high coefficient of determination ($R^2 = 0.87$). The Reynolds number, Re_b , characterizes the flow state at the canopy top. The lateral expansion of canopies shows a strong linear relationship with the Reynolds number, Re_b , with a high coefficient of determination ($R^2 = 0.80$).

The momentum exchange process in the mixing layer significantly increases with the lateral expansion of canopies at lower blockage levels. However, when the channel reaches a state of severe blockage, the momentum thickness approaches a constant value. We believed that the boundary friction effect plays a dominant role in the momentum exchange process near the wall, leading to distinct momentum exchange near the wall compared to other locations. This explanation finds strong support in the observation that the momentum thickness approaches a stable value when $B_r > 0.5$.

Rigid vegetation exhibits faster momentum exchange compared to flexible vegetation. Additionally, submerged vegetation exhibits vertical coherent vortex characteristics that emergent vegetation cannot demonstrate. Based on the previous findings, we have derived a relationship equation [Eq. (18)] that couples the vertical coherent vortex penetration length with the blocking ratio, and it exhibits a good fitting accuracy ($R^2 = 0.83$). With variations in blockage, the vertical coherent vortex penetration length shows a similar trend to the changes in the momentum thickness of the mixing layer, but the overall trend is not as extreme. The outer vortex will continue to evolve after the inner vortex reaches a stable state. High canopy density exhibits resistance to the penetration behavior of vertical coherent vortices. Indeed, the vertical scale and vortex penetration length have been validated by previous studies, providing ample justification for researching rigid vegetation.

ACKNOWLEDGMENTS

This research was supported by the National Natural Science Foundation of China (No. 52239006), the National Natural Science Foundation of Joint Fund for Changjiang River Water Science Research (No. U2340201), the Sichuan Science and

Technology Program (No. 2023NSFSC0283), the Open Research Fund of State Key Laboratory of Simulation and Regulation of Water Cycle in River Basin, the China Institute of Water Resources and Hydropower Research (Grant No. IWHR-SKL-KF202320), and the Open Foundation (Project Nos. SKHL2105 and SKHL2304), at State Key Laboratory of Hydraulics and Mountain River Engineering, Sichuan University.

AUTHOR DECLARATIONS

Conflict of Interest

The authors have no conflicts to disclose.

Author Contributions

Si-Yuan Song: Data curation (equal); Formal analysis (equal); Investigation (equal); Writing – original draft (equal). **Xie-Kang Wang:** Funding acquisition (equal). **Huan-Feng Duan:** Supervision (equal); Writing – review & editing (equal). **Alessandro Stocchino:** Writing – review & editing (equal). **Xu-Feng Yan:** Conceptualization (equal); Investigation (equal); Methodology (equal); Project administration (equal); Validation (equal); Writing – review & editing (equal).

DATA AVAILABILITY

The data that support the findings of this study are available from the corresponding author upon reasonable request.

APPENDIX: GRID INDEPENDENCE ANALYSIS

In this study, we analyzed the independence of the four numbers of grid cells, as shown in Fig. 15. When the grid cells are less than 27 200, the simulation accuracy of the non-vegetated area is more sensitive to the influence of grid size. When the number of grid cells is larger than 27 200, the range (R) = 0.0003, 0.0066, 0.0024, and 0.0019, as $y/b = 0.5, 0.9, 1.1$, and 1.5, respectively. It can

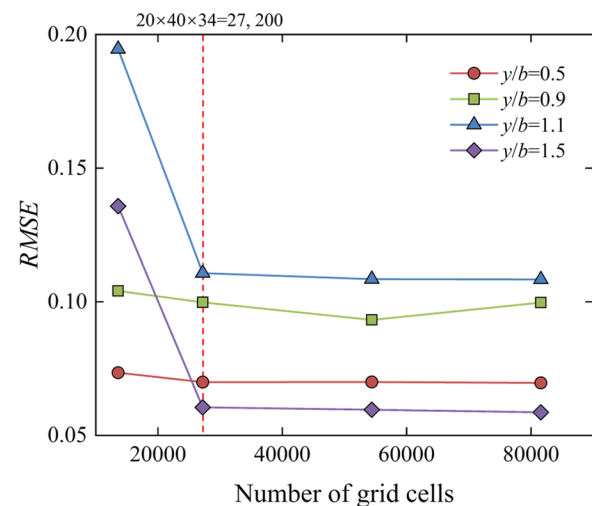


FIG. 15. Grid independence analysis. RMSE is the root mean square error between the numerical simulations and the experimental results under corresponding grids.

be clearly observed that there is almost no change in the *RMSE* at the same location. Further increase in grid cells has a limited effect on the simulation accuracy of the numerical model and also significantly improves the computational time, so 27 200 computational grid cells are used in this study, i.e., a grid corresponding to $21 \times 41 \times 35$ nodes. Intriguingly, we can also find that the numerical model used in this study has a lower simulation accuracy near the interface between vegetated and non-vegetated areas than at other locations, a result that is consistent with the description of the lower accuracy near the interface in the main text.

REFERENCES

- ¹J. Zhang, W. Wang, Z. Li, H. Wang, Q. Wang, and Z. Mi, "Evaluation of a random displacement model for scalar mixing in ecological channels partially covered with vegetation," *Environ. Sci. Pollut. Res.* **30**(11), 31281–31293 (2022).
- ²C. Liu, Y. Shan, W. Sun, C. Yan, and K. Yang, "An open channel with an emergent vegetation patch: Predicting the longitudinal profiles of velocities based on exponential decay," *J. Hydrol.* **582**, 124429 (2020).
- ³A. Vargas-Luna, G. Duró, A. Crosato, and W. Uijttewaalt, "Morphological adaptation of river channels to vegetation establishment: A laboratory study," *J. Geophys. Res.* **124**(7), 1981–1995, <https://doi.org/10.1029/2018JF004878> (2019).
- ⁴C. Camporeale, E. Perucca, L. Ridolfi, and A. M. Gurnell, "Modeling the interactions between river morphodynamics and riparian vegetation," *Rev. Geophys.* **51**(3), 379–414, <https://doi.org/10.1002/rog.20014> (2013).
- ⁵W. M. Van Dijk, R. Teske, W. I. Van De Lageweg, and M. G. Kleinhans, "Effects of vegetation distribution on experimental river channel dynamics," *Water Resour. Res.* **49**(11), 7558–7574, <https://doi.org/10.1002/2013WR013574> (2013).
- ⁶A. M. Carhart, J. E. Kalas, J. T. Rogala, J. J. Rohweder, D. C. Drake, and J. N. Houser, "Understanding constraints on submersed vegetation distribution in a large, floodplain river: The role of water level fluctuations, water clarity and river geomorphology," *Wetlands* **41**(5), 57 (2021).
- ⁷F. Sonnenwald, J. R. Hart, P. West, V. R. Stovin, and I. Guymer, "Transverse and longitudinal mixing in real emergent vegetation at low velocities," *Water Resour. Res.* **53**(1), 961–978, <https://doi.org/10.1002/2016WR019937> (2017).
- ⁸G. J. Vietz and B. L. Finlayson, "Geomorphological effects of flow alteration on rivers," in *Water for the Environment* (Elsevier, 2017), pp. 83–100.
- ⁹B. Doulatyari, S. Basso, M. Schirmer, and G. Botter, "River flow regimes and vegetation dynamics along a river transect," *Adv. Water Resour.* **73**, 30–43 (2014).
- ¹⁰Y.-Y. Jia, Z.-D. Yao, H.-F. Duan, X.-K. Wang, and X.-F. Yan, "Numerical assessment of canopy blocking effect on partly-obstructed channel flows: From perturbations to vortices," *Eng. Appl. Comput. Fluid Mech.* **16**(1), 1761–1780 (2022).
- ¹¹M. Ben Meftah and M. Mossa, "Partially obstructed channel: Contraction ratio effect on the flow hydrodynamic structure and prediction of the transversal mean velocity profile," *J. Hydrol.* **542**, 87–100 (2016).
- ¹²Z.-X. Xu, C. Ye, Y.-Y. Zhang, X.-K. Wang, and X.-F. Yan, "2D numerical analysis of the influence of near-bank vegetation patches on the bed morphological adjustment," *Environ. Fluid Mech.* **20**(4), 707–738 (2020).
- ¹³X. F. Yan, H. F. Duan, W. H. Onyx Wai, C. W. Li, and X. K. Wang, "Spatial flow pattern, multi-dimensional vortices, and junction momentum exchange in a partially covered submerged canopy flume," *Water Resour. Res.* **58**(3), e2020WR029494, <https://doi.org/10.1029/2020WR029494> (2022).
- ¹⁴T. Okamoto, I. Nezu, and H. Ikeda, "Vertical mass and momentum transport in open-channel flows with submerged vegetations," *J. Hydro-Environ. Res.* **6**(4), 287–297 (2012).
- ¹⁵M. Ghisalberti and H. M. Nepf, "Mixing layers and coherent structures in vegetated aquatic flows," *J. Geophys. Res.* **107**(C2), 3-1–3-11, <http://dx.doi.org/10.1029/2001JC000871> (2002).
- ¹⁶H. Nepf, M. Ghisalberti, B. White, and E. Murphy, "Retention time and dispersion associated with submerged aquatic canopies," *Water Resour. Res.* **43**(4), 2006WR005362, <https://doi.org/10.1029/2006WR005362> (2007).
- ¹⁷S.-U. Choi and H. Kang, "Numerical investigations of mean flow and turbulence structures of partly-vegetated open-channel flows using the Reynolds stress model," *J. Hydraul. Res.* **44**(2), 203–217 (2006).
- ¹⁸I. Kimura, S. Onda, T. Hosoda, and Y. Shimizu, "Computations of suspended sediment transport in a shallow side-cavity using depth-averaged 2D models with effects of secondary currents," *J. Hydro-Environ. Res.* **4**(2), 153–161 (2010).
- ¹⁹H. Shi, J. Zhang, and W. Huai, "Experimental study on velocity distributions, secondary currents, and coherent structures in open channel flow with submerged riparian vegetation," *Adv. Water Resour.* **173**, 104406 (2023).
- ²⁰H. M. Nepf and E. R. Vivoni, "Flow structure in depth-limited, vegetated flow," *J. Geophys. Res.* **105**(C12), 28547–28557, <https://doi.org/10.1029/2000JC900145> (2000).
- ²¹H. Widyayanti, E. O. Nugroho, A. S. Zulhaq, A. Zahroni, J. Nugroho, D. Harlan, A. Prasetyo, I. Soekarno, D. M. Samosir, A. S. B. Roesbianto, and Widyanyantias, "The effect of compound channel shape for local scouring and flow dynamics using NaysCUBE-3D RANS at Downstream Tukad Unda River Bali Province," *IOP Conf. Ser.* **1266**(1), 012012 (2023).
- ²²M. Cusipuma Ayuque and J. I. Montenegro Gambini, "Numerical investigation of 2D/3D hydrodynamic conditions in the proximity of a bridge in an Amazonian river," in The 25th EGU General Assembly, 2023.
- ²³S. Ali, T. Hosoda, and I. Kimura, "A non-linear κ - ϵ model to predict the spatial change of turbulent structures in large scale vortices," *J. Appl. Mech.* **10**, 723–732 (2007).
- ²⁴J. T. Rominger and H. M. Nepf, "Flow adjustment and interior flow associated with a rectangular porous obstruction," *J. Fluid Mech.* **680**, 636–659 (2011).
- ²⁵J. C. Green, "Comparison of blockage factors in modelling the resistance of channels containing submerged macrophytes," *River Res. Appl.* **21**(6), 671–686 (2005).
- ²⁶J. C. Green, "Effect of macrophyte spatial variability on channel resistance," *Adv. Water Resour.* **29**(3), 426–438 (2006).
- ²⁷B. L. White and H. M. Nepf, "Shear instability and coherent structures in shallow flow adjacent to a porous layer," *J. Fluid Mech.* **593**, 1–32 (2007).
- ²⁸M. Ben Meftah, F. De Serio, and M. Mossa, "Hydrodynamic behavior in the outer shear layer of partly obstructed open channels," *Phys. Fluids* **26**(6), 065102 (2014).
- ²⁹C. Yan, Y. Shan, W. Sun, C. Liu, and X. Liu, "Modeling the longitudinal profiles of streamwise velocity in an open channel with a model patch of vegetation," *Environ. Fluid Mech.* **20**(6), 1441–1462 (2020).
- ³⁰H. M. Nepf, "Flow and transport in regions with aquatic vegetation," *Annu. Rev. Fluid Mech.* **44**(1), 123–142 (2012).
- ³¹Y. Tanino and H. M. Nepf, "Laboratory investigation of mean drag in a random array of rigid, emergent cylinders," *J. Hydraul. Eng.* **134**(1), 34–41 (2008).
- ³²M. R. Raupach, P. A. Coppin, and B. J. Legg, "Experiments on scalar dispersion within a model plant canopy part I: The turbulence structure," *Boundary-Layer Meteorol.* **35**(1–2), 21–52 (1986).
- ³³X.-F. Yan, W.-H. Onyx Wai, and C.-W. Li, "Characteristics of flow structure of free-surface flow in a partly obstructed open channel with vegetation patch," *Environ. Fluid Mech.* **16**(4), 807–832 (2016).
- ³⁴M. Luhar, J. Rominger, and H. Nepf, "Interaction between flow, transport and vegetation spatial structure," *Environ. Fluid Mech.* **8**(5–6), 423–439 (2008).
- ³⁵Z. Chen, A. Ortiz, L. Zong, and H. Nepf, "The wake structure behind a porous obstruction and its implications for deposition near a finite patch of emergent vegetation," *Water Resour. Res.* **48**(9), 2012WR012224, <https://doi.org/10.1029/2012WR012224> (2012).
- ³⁶G. Calvani, C. Carbonari, and L. Solari, "Stability analysis of submerged vegetation patterns in rivers," *Water Resour. Res.* **58**(8), e2021WR031901, <https://doi.org/10.1029/2021WR031901> (2022).
- ³⁷C. Liu, Z. Hu, J. Lei, and H. Nepf, "Vortex structure and sediment deposition in the wake behind a finite patch of model submerged vegetation," *J. Hydraul. Eng.* **144**(2), 04017065 (2018).
- ³⁸H. M. Nepf, "Flow over and through biota," in *Treatise on Estuarine and Coastal Science* (Elsevier, 2011), pp. 267–288.
- ³⁹W. Huai, J. Zhang, G. G. Katul, Y. Cheng, X. Tang, and W. Wang, "The structure of turbulent flow through submerged flexible vegetation," *J. Hydrodyn.* **31**(2), 274–292 (2019).

- ⁴⁰N. Anjum and N. Tanaka, "Numerical investigation of velocity distribution of turbulent flow through vertically double-layered vegetation," *Water Sci. Eng.* **12**(4), 319–329 (2019).
- ⁴¹I. Nezu and K. Onitsuka, "Turbulent structures in partly vegetated open-channel flows with LDA and PIV measurements," *J. Hydraul. Res.* **39**(6), 629–642 (2001).
- ⁴²M. Ghisalberti and H. M. Nepf, "The limited growth of vegetated shear layers," *Water Resour. Res.* **40**(7), 2003WR002776, <https://doi.org/10.1029/2003WR002776> (2004).
- ⁴³I. Nezu and M. Sanjou, "Turbulence structure and coherent motion in vegetated canopy open-channel flows," *J. Hydro-Environ. Res.* **2**(2), 62–90 (2008).
- ⁴⁴C. Yan, H. M. Nepf, W.-X. Huang, and G.-X. Cui, "Large eddy simulation of flow and scalar transport in a vegetated channel," *Environ. Fluid Mech.* **17**(3), 497–519 (2017).
- ⁴⁵S.-U. Choi and H. Kang, "Characteristics of mean flow and turbulence statistics of depth-limited flows with submerged vegetation in a rectangular open-channel," *J. Hydraul. Res.* **54**(5), 527–540 (2016).
- ⁴⁶S.-Q. Yang, S.-K. Tan, and S.-Y. Lim, "Velocity distribution and diphenomenon in smooth uniform open channel flows," *J. Hydraul. Eng.* **130**(12), 1179–1186 (2004).
- ⁴⁷S. Moltchanov, Y. Bohbot-Raviv, and U. Shavit, "Dispersive stresses at the canopy upstream edge," *Boundary-Layer Meteorol.* **139**(2), 333–351 (2011).
- ⁴⁸Z.-R. Wang, S.-J. Zhang, Y.-X. Jiang, Z.-D. Yao, and X.-F. Yan, "Evaluating shallow mixing layer in partially-distributed canopy flows using DA-LES: Bed friction, water shallowness and canopy denseness," *Eng. Appl. Comput. Fluid Mech.* **18**(1), 2298075 (2024).
- ⁴⁹H. M. Nepf, "Hydrodynamics of vegetated channels," *J. Hydraul. Res.* **50**(3), 262–279 (2012).
- ⁵⁰J. D. Ackerman and A. Okubo, "Reduced mixing in a marine macrophyte canopy," *Funct. Ecol.* **7**(3), 305 (1993).
- ⁵¹M. Ghisalberti and H. Nepf, "The structure of the shear layer in flows over rigid and flexible canopies," *Environ. Fluid Mech.* **6**(3), 277–301 (2006).
- ⁵²Y. Shan, C. Yan, J. Liu, and C. Liu, "Predicting velocity and turbulent kinetic energy inside an emergent *Phragmites australis* canopy with real morphology," *Environ. Fluid Mech.* **23**(4), 943–963 (2023).
- ⁵³L. He, Y. Shan, C. Liu, H. Cao, X. Liu, and Y. Guo, "Prediction of bedload transport inside vegetation canopies with natural morphology," *J. Hydrodyn.* (published online) (2024).